Preparation of Magnetite Nanoparticles in Mesoporous Copolymer Template

ARTICLE *in* NANO LETTERS · FEBRUARY 2001

Impact Factor: 13.59 · DOI: 10.1021/nl005533k

NANO LETTERS

2001
Vol. 1, No. 2
105−108

Preparation of Magnetite Nanoparticles in Mesoporous Copolymer Template

D. Rabelo, E. C. D. Lima, and A. C. Reis

Universidade Federal de Goiás, Instituto de Química, CEP 74001-970, Goiânia-GO, Brazil

W. C. Nunes and M. A. Novak

Universidade Federal do Rio de Janeiro, Instituto de Física, CEP 21945-970, Rio de Janeiro-RJ, Brazil

V. K. Garg, A. C. Oliveira, and P. C. Morais*

Universidade de Brasília, Instituto de Física, CEP 70919-970, Brasília-DF, Brazil

Received December 18, 2000

ABSTRACT

Preparation of size-controllable magnetite (Fe_3O_4) nanoparticles by alkaline oxidation of ferrous ion adsorbed in sulfonated mesoporous styrene−divinylbenzene copolymer is described. It was observed that the magnetite nanoparticle size increases by ion-charging the sulfonated polymeric template with ferrous aqueous solution at increasing iron concentration. A simple model describing the amount of iron incorporation in the polymeric template is proposed. The magnetite-based composite was investigated by atomic absorption, transmission electron microscopy, Mössbauer spectroscopy, X-ray diffraction, and magnetization data.

In recent years the technique known as high-gradient magnetic separation (HGMS) has been attracting a great deal of attention.[1−6] Applications of such a technique span from cell separation[1] to removal of actinides from wastewater.[2] The HGMS technique uses nanosized magnetic particles that are surface-coupled to the target species for removal of the latter by using a high-gradient magnetic field device.[3,4] Magnetite (Fe_3O_4) nanoparticles, surface-coated either with a nonspecific[5] or specific[6] molecular layer, have been widely used in HGMS. In addition to specificity, the coating molecular layer prevents magnetite nanoparticles from oxidation toward a lower saturation magnetization iron oxide phase. Stable magnetite-based composites may be physically and chemically engineered to support cleanup remediation technologies addressed to water oil spills in natural environments using HGMS-based processes.

Copolymer templates have been used in the production of iron oxide nanomagnetic crystallites.[7−10] Polymer morphology and chemical treatment, however, strongly affect the nature of the final iron oxide phase. Alkaline oxidation of Fe^{2+} in gel-typed sulfonated polystyrene was used to obtain maghemite (γ-Fe_2O_3) nanoparticles.[7] Oxidation of Fe^{2+} in macroporous sulfonated cross-linked polystyrene produces superparamagnetic goethite (FeOOH),[8] while a mixture of maghemite and goethite nanoparticles is obtained in mesoporous sulfonated cross-linked polystyrene.[9] Magnetite nanoparticles were successfully prepared by using polystyrene−polyacrylate copolymer gel as template.[10] In this study, mesoporous sulfonated styrene−divinylbenzene (Sty−DVB) copolymer template was used to produce stable and size-controllable magnetite (Fe_3O_4) nanoparticles. For over six months the magnetite-based composite samples have been immersing in water with no visible oxidation to maghemite. Furthermore, the size-control of the magnetite particle has been successfully achieved through the control of the ferrous ion concentration incorporated in the polymeric template. Atomic absorption, transmission electron microscopy (TEM), Mössbauer spectroscopy, X-ray diffraction, and magnetization data were used to characterize the magnetite-based composite.

Micron-sized spheres of mesoporous Sty−DVB copolymer were produced by suspension polymerization in the presence of inert diluents, as described elsewhere.[11] The dried polymeric template was characterized by the apparent density (0.44 g/cm^3), surface area (140 m^2/g), average pore diameter (13 nm), toluene regain (1.52 cm^3/g), heptane regain (1.24 cm^3/g), % volume swelling in toluene (100), and % volume swelling in heptane (58). The mesoporous copolymer was

* Corresponding author. Telephone number: (+55-61) 273-6655. Fax number: (+55-61) 272-3151. E-mail address: pcmor@fis.unb.br.

10.1021/nl005533k CCC: $20.00
Published on Web 01/27/2001

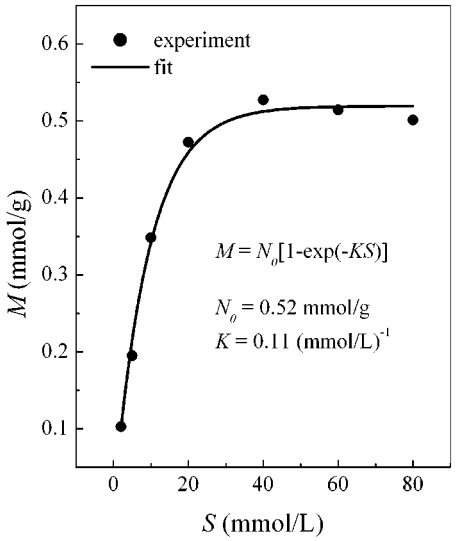

Figure 1. Total iron incorporation in the polymeric template (M) versus ferrous iron concentration of the bath solution (S).

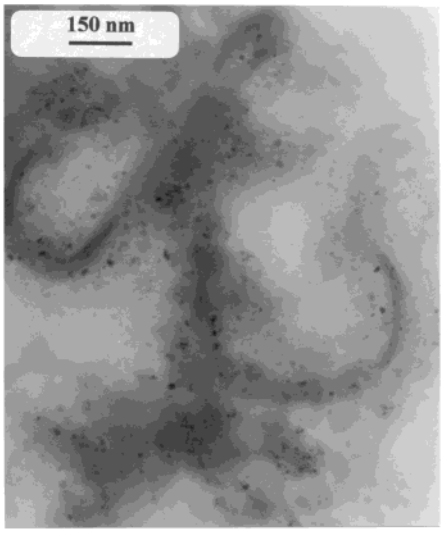

Figure 2. TEM micrograph of the 2 mmol/L composite sample.

sulfonated using concentrated sulfuric acid (97%). The reaction was carried out in the presence of dichloroethane (40% in volume with respect to sulfuric acid). Composites were prepared using the micron-sized sulfonated template immersed in $FeSO_4$ aqueous solution (bath solution) at different Fe^{2+} concentrations ($S = 2$, 5, 10, 20, 40, 60, and 80 mmol/L). The preparation follows a three-step procedure. First, the mixture was stirred for 1 h at room temperature. Second, the polymer particles were separated by filtration and washed thoroughly with water until no iron was detected in the eluent (*o*-phenanthroline test). Third, oxidation of the Fe^{2+} was performed in alkaline medium. The iron-containing resin was immersed in the oxidizing solution (aqueous solution containing KOH and $NaNO_3$). The oxidation procedure realized in this study is the standard recipe used in the synthesis of magnetite microcrystals from Fe^{2+} in aqueous solution.[12] The obtained black magnetic composite was filtered, washed with water until the pH of the eluent was neutral, and dried in an oven at 60 °C for 2 h.

The total iron content of the composite sample was determined using a Perkin-Elmer 5000 atomic absorption equipment. Full circles in Figure 1 show the total iron incorporation (M) in the template after performing the oxidation step, in units of millimole of iron per unit gram of the initial copolymer template, as a function of ferrous concentration (S) in the bath solution. The data shown in Figure 1 were analyzed in terms of a simple ion incorporation model. The model describes iron incorporation as a result of the first two steps of the preparation process. The first step represents the copolymer ferrous charge, while the second step accounts for the partial ferrous discharge. After ion diffusion into the copolymer template and the steady-state concentration is achieved, iron ion will be found in three different environments, namely, the left aqueous iron in the bath solution, iron ion inside the template nanocavity but bonded to a sulfonic-like active site, and aqueous iron inside the polymer nanocavity. As long as the sulfonic-like active site concentration is higher than the sulfonic-bonded iron ion concentration, the rate at which iron is incorporated in the polymer template, driven by iron ion concentration (S), i.e., dM/dS, can be given by $K(N - M)$. Note that K represents a characteristic parameter that describes the adsorption of aqueous iron by the mesoporous polymeric template, while N represents the maximum ferrous ion incorporation. Therefore, M versus S can be obtained by solving the differential equation $dM/dS = K(N - M)$, i.e., $M = N[1 - \exp(-KS)]$. However, before alkaline oxidation is performed (third step) a partial ferrous ion desorption occurs due to the washing procedure (second step). It is assumed that, at the end of the second step, N is reduced to $N_0 = \lambda N$, where $\lambda < 1$ represents the degree of ferrous ion desorption. The solid line in Figure 1 represents the best fit of the experimental data using the solution of the above-mentioned differential equation, taking into account the partial ferrous ion desorption, i.e., the expression $M = N_0[1 - \exp(-KS)]$, with $N_0 = 0.52$ mmol/g and $K = 0.11$ (mmol/L)$^{-1}$. Note that 1 mmol/g in the vertical scale (Figure 1) represents about 7.2 wt % of magnetite in the composite. In addition, as the ion exchange capacity of the polymeric template is 4.8 mmol H^+/g,[13] the ratio of sulfonic group/iron incorporation spans from about 0.2 ($S = 2$ mmol/L) to 1 ($S = 80$ mmol/L).

Figures 2 and 3 show the TEM (bright field mode) of the $S = 2$ and 20 mmol/L composite samples, respectively. Parts a and b of Figure 4 show the particle size histograms (about 150 total counts each) obtained from the TEM images of the $S = 2$ and 20 mmol/L composite samples, respectively. The particle size histogram in Figure 4a was curve fitted using the log-normal probability function,[14] from which the average particle diameter and standard deviation were $\langle D \rangle = 8$ nm and $\sigma = 0.36$, respectively. Likewise, the fitting of the particle size histogram shown in Figure 4b gives $\langle D \rangle = 50$ nm and $\sigma = 0.31$.

Low-temperature (77 K) transmission Mössbauer spectra were recorded using an MCA (256 channels) and a Wissel constant acceleration transducer coupled to a 50 mCi ^{57}Co/Rh source. Mössbauer spectra of the composite samples (see

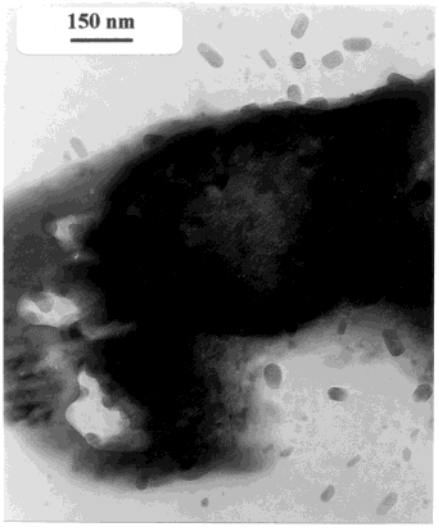

Figure 3. TEM micrograph of the 20 mmol/L composite sample.

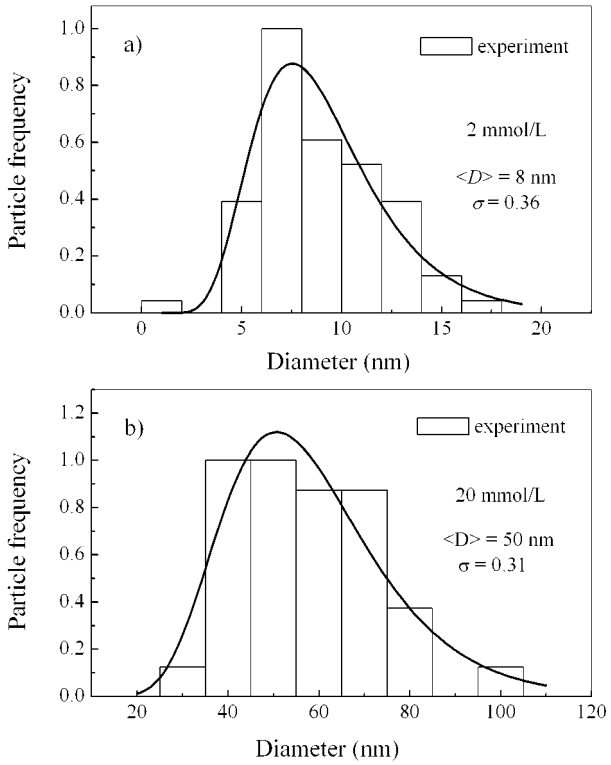

Figure 4. Particle size histogram (TEM data) of magnetite particles in the (a) 2 mmol/L composite sample and (b) 20 mmol/L composite sample.

Figure 5) were resolved for two sextets with internal magnetic fields in the range 510−518 kOe (Fe^{3+} tetrahedral A-site) and 487−499 kOe (Fe^{2+}/Fe^{3+} octahedral B-site). These values are reasonably close to the reported values for bulk magnetite,[15] ideal composition, $Fe^{3+}[Fe^{2+}Fe^{3+}]O_4$. The corresponding room-temperature Mössbauer spectra (data not shown) were also resolved for two sextets with internal fields close to the values reported for bulk magnetite, indicating that magnetic ordering is effective even for the smallest nanoparticle investigated ($S = 5$ mmol/L).

In support of the Mössbauer data that indicate magnetite as the main iron oxide phase, Figure 6 shows the X-ray

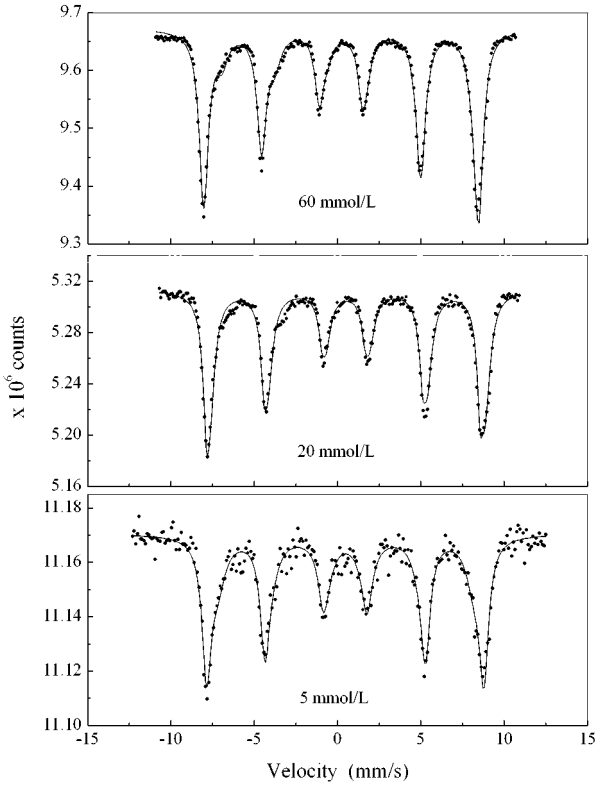

Figure 5. Low-temperature Mössbauer spectra of the $S = 5$, 20, and 60 mmol/L composite samples. Full circles are the experimental data while the solid lines represent the best fit with two sextets.

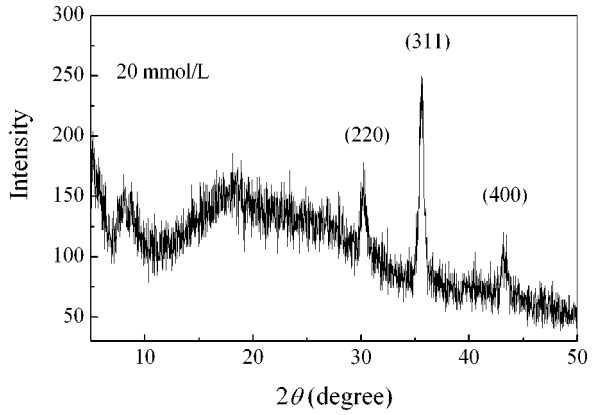

Figure 6. X-ray diffraction of the 20 mmol/L composite sample.

diffraction data of the $S = 20$ mmol/L composite sample. The peak position (relative intensity) of the (220), (311), and (400) lines of the sample are 30.224° (29.8), 35.606° (100), and 43.227° (18.9), while the ASTM data of magnetite are 30.122° (30), 35.455° (100), and 43.099° (20), respectively.

Finally, room-temperature magnetization (m) of the $S = 10$ mmol/L composite sample was obtained, as shown in Figure 7 (full circles). The solid line in Figure 7 represents the best fit of the $S = 10$ mmol/L data according to the following equation $m(H;\langle D\rangle,\sigma) = m_0 \int L_1(H,D)\ P(D)\ \mathrm{d}D$, where $L_1(H,D) = \coth(\xi) - (1/\xi)$ is the first-order Langevin function, $P(D)$ is the log-normal probability function, $m_0 = \phi m_S$ is the composite saturation magnetization, ϕ is the magnetite volumetric fraction in the composite, and m_S is the bulk magnetite saturation magnetization (470 G). Note

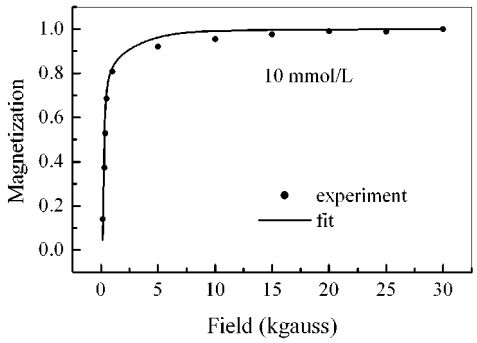

Figure 7. Room-temperature magnetization of the 10 mmol/L composite sample.

that $\xi = \mu H/kT$, with $\mu = m_s V = (\pi/6)m_s D^3$. The model described by $m(H;\langle D\rangle,\sigma)$ is the traditional one, used to unfold the particle size polydispersity in nanomagnetic-based materials.[16] The particle size distribution obtained from the fitting of the magnetization data, averaged out by the log-normal distribution function, gives $\langle D\rangle = 19$ nm and $\sigma = 0.33$. In Figure 7 full circles are slightly below the solid line, indicating that particle−particle interaction needs to be included for more detailed analysis.

In summary, the characteristics of the iron oxide-based composite obtained in this study, in comparison to the literature,[7−10] show that the synthesized iron oxide phase depends not only upon the template structure but also upon the oxidation condition. The same oxidation recipe used to obtain magnetite microcrystals from aqueous ferrous solution[12] was employed in this study to produce size-controllable magnetite nanoparticles in a mesoporous polymer template. Atomic absorption data indicate that the total iron incorporation (M) increases until saturation as the ferrous ion concentration in the bath solution (S) increases. Transmission electron microscopy was used to obtain the magnetite particle size polydispersity profile in the polymer template. Mössbauer spectroscopy was used to characterize the synthesized iron oxide phase. X-ray diffraction data obtained from the $S = 20$ mmol/L composite sample are in excellent agreement with the standard data of magnetite (ASTM data). Saturation magnetization measurement of the $S = 10$ mmol/L (470 G) not only supports the magnetite phase but is used to unfold the particle size distribution. Combination of the iron incorporation data with the average nanoparticle size (from TEM and magnetization) may help to shine some light upon the growth process. The ratio $M/\langle D\rangle^3$ decreases as S increases, indicating reduction of the total number of particles as D increases. Such a trend may also indicate that magnetite nanoparticles are preferentially formed inside the porous instead of in the organic matrix, as has been reported in the case of the polystyrene−polyacrylate template.[10] Besides the magnetite synthesis using a mesoporous polymeric template, the most striking result of the present study is the nanosize-control possibility, via the amount of ferrous ion incorporated in the sulfonated polymeric template prior to the oxidation step. Indeed, a simple mass-charging model describes the incorporation of ferrous ion in the sulfonated polymeric template as a function of the total iron concentration in the bath solution. Stability of the magnetite nanoparticles against oxidation toward maghemite plus the possibility to control the size/amount of magnetic nanoparticles incorporated in the polymeric template make the obtained composite a good candidate for HGMS of water−oil emulsions. Nevertheless, the mechanism through which magnetite nanoparticles are formed under the conditions reported in this study is still an open question.

Acknowledgment. This work was partially supported by the Brazilian Agencies CTPetro, CNPq, FUNAPE-UFG, PRONEX, and FAP-DF. We thank NITRIFLEX for supplying monomers used in this study.

References

(1) Honda, H.; Kawabe, A.; Shinkai, A.; Kobayashi, T. J. *J. Ferment. Bioeng.* **1998**, *86*, 191.
(2) Ebner, A. D.; Ritter, J. A.; Ploehn, H. J.; Kochen, R. L.; Navratil, J. D. *Sep. Sci. Technol.* **1999**, *34*, 1277.
(3) Sun, L. P.; Zborowski, M.; Moore, L. R.; Chalmers, J. J. *Cytometry* **1998**, *33*, 469.
(4) Kurinobu, S.; Uesugi, J.; Utumi, Y.; Kasahara, H. *IEEE Trans. Magn.* **1999**, *35*, 4067.
(5) Bulte, J. W. M.; Ma, L. D.; Magin, R. L.; Kamman, R. L.; Hulstaert, C. E.; Go, K. G.; The, T. H.; Deleij, L. *Magn. Reson. Med.* **1993**, *29*, 32.
(6) Iinuma, H.; Okinaga, K.; Adachi, M.; Suda, K.; Sekine, T.; Sakagawa, K.; Baba, Y.; Tamura, J.; Kumagai, H.; Ida, A. *Int. J. Cancer* **2000**, *89*, 337.
(7) Ziolo, R. F.; Giannelis, E. P.; Weinstein, B. A.; O'Horo, M. P.; Ganguly, B. N.; Mehrotra, V.; Russell, M. W.; Huffman, D. R. *Science* **1992**, *257*, 219.
(8) Winnik, F. M.; Morneau, A.; Ziolo, R. F.; Stöver, H. D. H.; Li, W.-H. *Langmuir* **1995**, *11*, 3660.
(9) Winnik, F. M.; Morneau, A.; Mika, A. M.; Childs, R. F.; Roig, A.; Molins, E.; Ziolo, R. F. *Can. J. Chem.* **1998**, *76*, 10.
(10) Breulmann, M.; Colfen, H.; Hentze, H. P.; Antonietti, M.; Walsh, D.; Mann, S. *Adv. Mater.* **1998**, *10*, 237.
(11) Coutinho, F. M. B.; Rabelo, D. *Eur. Polym. J.* **1992**, *257*, 219.
(12) Couling, S. B.; Mann, S. *J. Chem. Soc., Chem. Commun.* **1985**, 1713.
(13) Helfferich, F. *Ion Exchange*; McGraw-Hill: New York, 1962.
(14) Rowel, R. L.; Levit, A. B. *J. Colloid Interface Sci.* **1970**, *34*, 585.
(15) Kuzmann, E.; Nagy, S.; Vértes, A.; Weiszburg, T. G.; Garg, V. K. Geological and Mineralogical Applications of Mössbauer Spectroscopy. In *Mineralogy and Geology−Techniques and Applications*; Vértes, A., Nagy, S., Süvegh, K., Eds.; Plenum Press: New York, 1998; p 285.
(16) Morais, P. C.; Lacava, B. M.; Bakuzis, A. F.; Lacava, L. M.; Silva, L. P.; Azevedo, R. B.; Lacava, Z. G. M.; Buske, N.; Nunes, W. C.; Novak, M. A. *J. Magn. Magn. Mater.*, in press.

NL005533K